




THE PROGRESS OF ^{14}C -AMS ANALYSIS FOR ULTRA-SMALL SAMPLES AT XI'AN AMS CENTER

Hua Du^{1,2*}  • Yunchong Fu^{1,2,4*} • Peng Cheng^{1,2,4}  • Haiyan Zhao^{2,3}  • Yaoyao Hou^{1,2} • Xiaohu Xiong^{1,2} • Huachun Gu^{2,3} • Ling Yang^{1,2}

¹State Key Laboratory of Loess and Quaternary Geology, Institute of Earth Environment, Chinese Academy of Sciences, Xi'an 710061, China

²Shaanxi Key Laboratory of Accelerator Mass Spectrometry Technology and Application, Xi'an AMS Center, Xi'an 710061, China

³Xi'an Institute for Innovative Earth Environment Research, Xi'an 710061, China

⁴Institute of Global Environmental Change, Xi'an Jiaotong University, Xi'an 710049, China

ABSTRACT. As there exists a growing demand for chronological research and tracer applications using radiocarbon (^{14}C) analyses of samples smaller than 100 $\mu\text{g C}$, a compact micro-specific hydrogen graphitization method has been developed at the Xi'an Accelerator Mass Spectrometry (AMS) Center. This article describes the performance of the system and the mass of carbon background produced during ultra-small sample preparation. Furthermore, we discuss the results of contamination corrections and perform ^{14}C analyses on small samples with known age or reference values. The results reveal that our ^{14}C analysis of ultra-small samples of 10–100 $\mu\text{g C}$ can obtain accurate and reliable results, and the micro-scale ^{14}C -AMS analysis technique meets our research objectives for dating and tracer applications.

KEYWORDS: AMS, graphitization reactor, radiocarbon background correction, radiocarbon, ultra-small samples.

INTRODUCTION

In recent years, there has been an increase in demand for radiocarbon (^{14}C) analyses of samples with less than 100 micrograms of carbon ($\mu\text{g C}$) with continuous improvement of single-molecule separation technologies and the expansion of new ^{14}C applications. These currently include the use of anthropogenic signals from nuclear testing (^{14}C bomb peak) (Cook et al. 2006; Buchholz and Spalding 2010; Saitoh et al. 2019), compound-specific radiocarbon analysis (CSRA), for environmental (Eglinton et al. 1996; Zhao et al. 2014; Druffel et al. 2010; Feng et al. 2017; Zhang et al. 2021) and archaeological samples (Berstan et al. 2008; Devière et al. 2018; Casanova et al. 2020; Spindler 2021); in-situ ^{14}C measurements (Lifton et al. 2001; Miller et al. 2006; Pigati et al. 2010; Lupkera et al. 2019; Hippe et al. 2009, 2021); and biomedical applications (Salehpour et al. 2013; Spalding et al. 2008, 2013), all these employ micro-scale ^{14}C -AMS analyses. This increasing demand for ultra-small samples has prompted the development of specialized graphitization techniques and other approaches. Micro-scale ^{14}C -AMS analysis will pave the way for challenging analysis relevant to chronological research and tracer applications.

Since the late 1990s, several AMS laboratories have developed techniques and used them for micro-scale ^{14}C analysis. For example, the Keck Carbon Cycle Accelerator Mass Spectrometry laboratory at the University of California, Irvine (KCCAMS/UCI) has developed sample preparation, measurement setup, data analysis, and background corrections for ultra-small mass ^{14}C -AMS (1000–2 $\mu\text{g C}$) (Santos et al. 2007a, 2007b, 2010; Xu et al. 2013; Walker and Xu 2019). In routine ^{14}C analysis at the National Ocean Sciences Accelerator Mass Spectrometry (NOSAMS) laboratory, a minimum sample mass of 25 $\mu\text{g C}$ has been achieved, and ultra-small graphitization reactors have been developed (Pearson et al. 1998; Walter et al. 2015). By 2004, the Australian Nuclear Science and Technology Research Organization (ANSTO) laboratory

*Corresponding authors. Emails: duhua@ieecas.cn and fuyc@ieecas.cn



routinely analyzed ^{14}C samples less than 100 $\mu\text{g C}$, using a 2.5 mL micro-specific hydrogen graphitization reactor for samples with 10–200 $\mu\text{g C}$. Subsequently, they developed a novel miniaturized laser-heated “microfurnace” aimed at preparing ultra-small mass ($\sim 5 \mu\text{g C}$) graphite samples from carbon dioxide (CO_2) (Hua et al. 2004; Smith et al. 2006, 2010; Yang and Smith 2017). Scientists at Tokyo University have developed the most optimal conditions for ultra-small ^{14}C samples (5–400 $\mu\text{g C}$) measurements by improving the pretreatment method to reduce modern and ^{14}C -dead carbon contamination and optimizing the graphite position in the target holders to maximize beam intensity (Yokoyama et al. 2010; Yamane et al. 2019). At the Vienna Environmental Research Accelerator (VERA) laboratory, AMS measurement performance on micrograms of graphite has also been explored (Liebl et al. 2013; Steier et al. 2017). Moreover, several laboratories have measured small $^{14}\text{CO}_2$ gas samples using EA-AMS online coupling technology (Ruff et al. 2007, 2010; Uhl et al. 2007; Fahrni et al. 2013; Welte et al. 2018; Melchert et al. 2019).

Small-mass radiocarbon samples ($>25 \mu\text{g C}$) are now routinely analyzed at the Xi'an AMS facility (Fu et al. 2015). However, ultra-small samples require further development, with a dedicated graphitization reactor and systematic study of reproducibility and background for ^{14}C analysis. The Xi'an AMS Center has installed new micro hydrogen graphitization reactors that were made at ANSTO. The goals of our study are: (1) to report on the performance of micro-specific graphitization reactors and ^{14}C -AMS measurements of small to ultra-small samples, (2) to evaluate and correct the carbon contamination during sample preparation and analysis, (3) to assess the reproducibility and accuracy of our micro-scale ^{14}C -AMS analysis, (4) to perform a case study about the chronological application on ^{14}C -AMS analysis of small foraminiferal samples.

SAMPLE PREPARATION AND AMS MEASUREMENTS

The Micro-Specific Graphitization Reactor

The micro-specific graphitization reactors are based on the micro conventional furnace (MCF) design at ANSTO (Yang et al. 2013; Yang and Smith 2017). The MCF is a cost-effective solution for producing graphite from carbon dioxide sample gas and is connected to a vacuum line for the synthesis of graphitic carbon in 1.2 mL fixed reaction tubes using hydrogen reduction. Reducing the internal volume of reactors is an effective approach for graphitizing smaller samples while minimizing isotopic fractionation (Pearson et al. 1998; Santos et al. 2007; Yokoyama et al. 2010). Our device comprises two small-volume graphitization reactors connected by quartz manifolds and stainless steel cold fingers suitable to trap water vapor during the reaction. Samples with 10–300 $\mu\text{g C}$ can be synthesized in a tube furnace at 600°C, adding reduced iron powder and ultrapure hydrogen (H_2), these reactors can also produce a few micrograms of graphite ($<10 \mu\text{g C}$).

The performance of the micro-specific graphitization reactors was assessed by analyzing ultra-small standard samples, including the National Institute of Standards and Technology (NIST) standard oxalic acid II (OxII; SRM 4990C) as well as secondary standards - International Atomic Energy Agency (IAEA) ^{14}C reference materials (IAEA-C2, IAEA-C3, IAEA-C6, IAEA-C7) and background samples (calcite, Sigma Aldrich graphite, 99.99% pure, -100 mesh, anthracite, CO_2 background gas). Many smaller CO_2 standard gases were obtained by combustion or hydrolyzed of large quantities of the standard materials with 85% orthophosphoric acid (H_3PO_4) and subsampled to equal 5–150 $\mu\text{g C}$ for graphite synthesis on the ultra-small reactors.

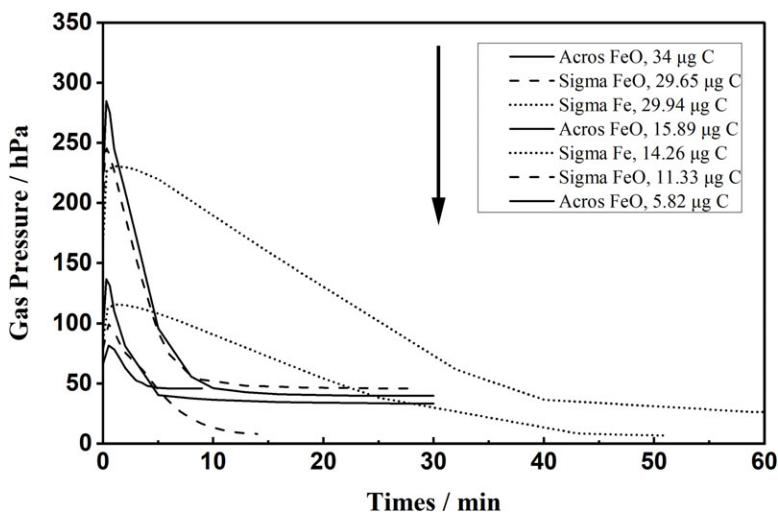


Figure 1 Graphitization reaction curves for a variety of CO₂ gases with varying carbon size catalyzed by various Fe reagents. The solid line for Acros FeO, the dashed line for Sigma FeO, and the dotted line for Sigma Fe are used to depict the three Fe catalysts, and the carbon size is decreased sequentially from top to bottom.

Performance of Micro-Specific Graphitization Reactors

We analyzed the effects of different catalysts and reducing agents involved in the graphitization of microgram carbon samples based on Scanning electron microscope (SEM) images and AMS measurements to determine appropriate conditions for the synthesis of ultra-small mass graphite.

Efficiency of Graphitization with Different Fe Catalysts

Hydrogen-catalyzed reduction reactions were conducted using four Fe catalysts: (1) Sigma FeO: Fe₂O₃ powder (Sigma Aldrich, ≥99.995% pure), (2) Acros FeO: Fe₂O₃ powder (Acros organics, 99.999% pure, -100 mesh), (3) Sigma Fe: Fe powder (Sigma Aldrich, 97% pure, -325 mesh), and (4) nano FeO: Fe₂O₃ powder. These Fe catalysts were processed by first reducing Fe or Fe₂O₃ in H₂ at 600°C before graphitization. Subsequently, AMS measurement and micro-scale morphological analyses were conducted to determine optimal reagents. This section aims to establish the optimal reagents and suitable mass of carbon for micro-specific graphitization reactors by synthesizing and analyzing graphite samples with different carbon masses.

First, we examined the graphitization reaction curves of CO₂ gas samples with various carbon masses using the four different Fe catalysts described above. The reaction curves for the first three Fe catalysts are shown in Figure 1 as residual gas pressure during graphitization. Nano-FeO is not shown due to low yields (20–30%). Sample masses in Figure 1 range from 34–5.82 µg C. “0” on the time-scale in Figure 1 denotes the moment when the graphitization reaction tube was pushed into the 600 °C furnace, indicating the warming up period before the graphitization reaction, during which the gas pressure first rises rapidly due to the temperature increase. All of the curves reach a peak within one minute. From this point, the pressure of all the gases begins to drop, which means the true beginning of all graphitization reactions, two types of curves are observed: (1) a rapid graphitization that is completed within 15 minutes (Acros FeO and Sigma

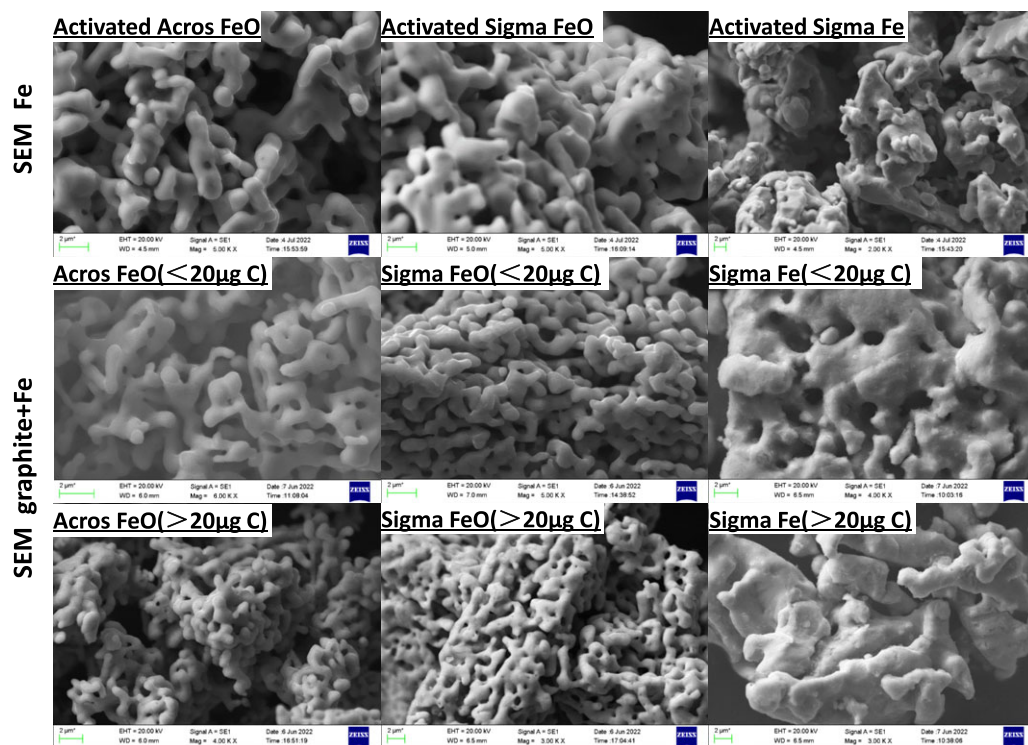


Figure 2 The SEM images of iron powder before and after graphitization.

FeO); and (2) a relatively slow graphitization that is completed within 45 minutes (Sigma Fe). The reaction time also depends on the sample mass. A sample with 5 μg C can be processed in five minutes. We conclude that Acros FeO and Sigma FeO have the highest efficiency with nearly 100% reaction yields.

SEM Morphological Analysis of Different Fe Catalysts

Sigma Fe catalyst is used routinely at the Xi'an lab for graphitization in standard ^{14}C analyse. However, for ultra-small samples, FeO catalysts appear to perform better. SEM analysis of graphites produced in our experiments was performed on the Fe catalysts and Fe-C mixtures using a Zeiss EVO18 multipurpose SEM analysis system. The results are shown in Figure 2 with 2- μm resolution. Graphite for these tests was synthesized from the IAEA-C2 reference standard with carbon mass above and below 20 micrograms. Another graphite with a similar C mass was synthesized and measured by AMS to measure $^{12}\text{C}^{3+}$ currents and fraction modern C ($F^{14}\text{C}$) values. SEM images of several activated Fe powders revealed that most exhibit relatively smooth surfaces with both types of FeO. These showed a relatively large surface area, as compared to Sigma Fe which may explain the relatively slow reaction time of the latter.

A black graphite-coated iron powder is produced during the graphitizations and this form contributes to strong and reliable ion currents for AMS analysis along with accurate and precise $F^{14}\text{C}$ values (Kim et al. 2008). Although the mass of carbon is small, a visible amount of graphite was observed on the surface of Fe powder in the SEM images (Figure 2), no apparent difference exists between the images of different carbon masses, however, $^{12}\text{C}^{3+}$ beam current

and $F^{14}\text{C}$ values (reference value: 0.4114 ± 0.0003) of the IAEA-C2 reference standard targets measured by AMS were significantly different. All the targets $>20 \mu\text{g C}$ had relatively high $^{12}\text{C}^{3+}$ currents and $F^{14}\text{C}$ values close to their reference values, whereas all the targets $<20 \mu\text{g C}$ produced relatively low $^{12}\text{C}^{3+}$ currents and $F^{14}\text{C}$ values, further from their reference values. Based on the SEM images, Sigma FeO and Acros FeO catalysts appear to be better than Sigma Fe (based on surface area), and they outperformed Sigma Fe, based on reaction rate analysis, with varying carbon sizes.

The Sigma FeO catalyst was selected as our catalyst of choice since it demonstrated superior reaction rates and consistent $F^{14}\text{C}$ values for samples $<20 \mu\text{g C}$. With this dedicated trace graphitization system, all CO_2 gas samples above $5 \mu\text{g C}$ can be synthesized, and the optimal amount of carbon for the analyzed samples lies within the range of $10\text{--}200 \mu\text{g C}$.

AMS Measurements

All samples were analyzed using the 3 MV multi-nuclide Accelerator Mass Spectrometer at the Xi'an AMS Center, Institute of Earth Environment, Chinese Academy of Sciences. Under routine ion source conditions producing $\sim 20 \mu\text{A } ^{12}\text{C}^-$ from graphite injected into the tandem accelerator, the ion injection energy used was 35 k eV, and a fast 100 Hz cycling frequency was routinely employed in the Fast Sequential Injection (FSI) mode that alternates $^{12}\text{C}^-$, $^{13}\text{C}^-$ and $^{14}\text{C}^-$ injections. The isotopes: ^{12}C , ^{13}C , $^{14}\text{C}^{3+}$ were measured in the high-energy end of the machine with a terminal voltage of 2.5 MV. The best background of $^{14}\text{C}/^{12}\text{C}$ was 1.84×10^{-16} with a long-term daily $^{14}\text{C}/^{12}\text{C}$ procedural background range for 1 mg C in the range of 9×10^{-16} to 2×10^{-15} (Figure 3; Zhou et al. 2006, 2007, 2012).

According to the carbon mass of samples, the analyzed graphite samples were divided into wheels of $>20 \mu\text{g C}$ targets and $<20 \mu\text{g C}$ targets, and targets with activated Fe_2O_3 , Fe powder, and Nd powder were inserted into each batch of samples to monitor ^{14}C counting interference. Sample batches consist of a set of small standards with the same size as the unknown samples, analyses of IAEA reference materials and background materials of the same type as unknown samples, as well as OxII standards that are used for quality and consistency control and standards normalization. Measured $^{14}\text{C}/^{12}\text{C}$ ratios are reported as $F^{14}\text{C}$. The data were analyzed and performed the correction for isotope fractionation (normalization to $\delta^{13}\text{C} = -25\text{‰ VPDB}$). Uncertainties of our data are fully propagated for each correction.

AMS RESULTS AND DISCUSSION

Beam Current Investigation

Figure 4 shows the $^{12}\text{C}^{3+}$ beam currents that we measured on the AMS. The $^{12}\text{C}^{3+}$ beam current intensity of 1 mg C samples was $20\text{--}30 \mu\text{A}$ and decreased to a few μA or even below $1 \mu\text{A}$ as the carbon mass of the sample decreased (Figure 4). In general, we fix the C/Fe mass ratio for conventional mg-scale samples to 1:2 (Zn method) or 1:3 (H_2 method). To make it easier to load ultra-small mass samples into the holder, we used a constant amount of iron (1 mg Fe or 1.43 mg Fe_2O_3) regardless of carbon mass. Hence, the C concentration in the targets decreases with carbon mass. This dilution caused the $^{12}\text{C}^{3+}$ beam current to decrease with decreasing sample mass. We achieved a maximum $^{12}\text{C}^{3+}$ beam currents of approximately $0.1 \mu\text{A}$ per μg of carbon. The carbon concentration in conventional 1 mg graphite targets was about 25% (calculated by the C/Fe mass ratio of 1:3), corresponding to an anion beam current of $20\text{--}30 \mu\text{A}$. For samples of $200 \mu\text{g C}$ or more, the $^{12}\text{C}^{3+}$ beam current was stable and above $20 \mu\text{A}$, which is consistent with

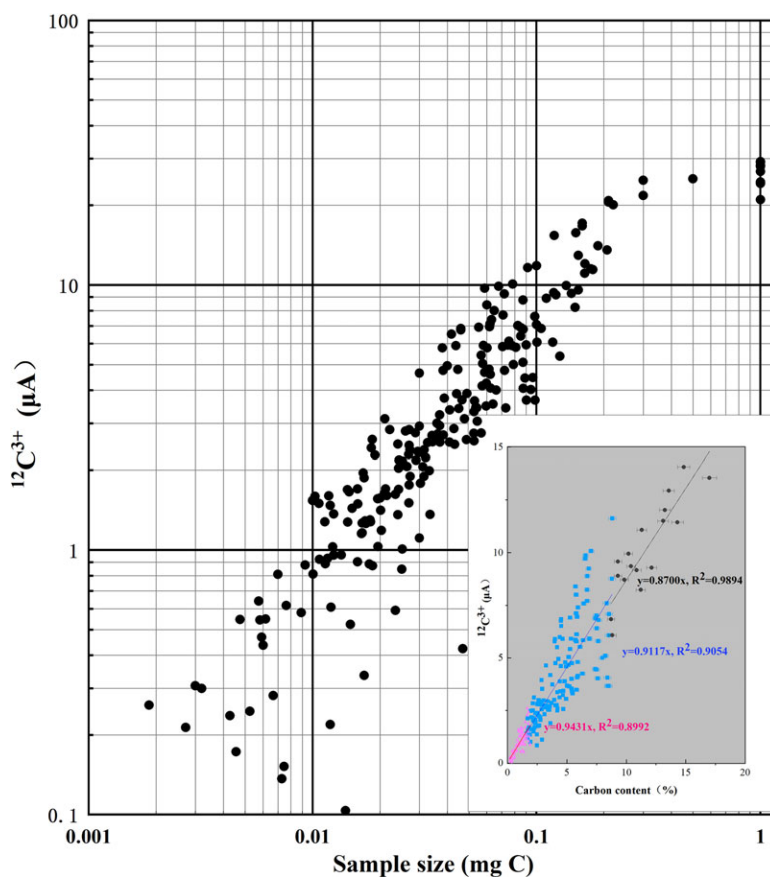


Figure 3 Plot of the average $^{12}\text{C}^{3+}$ beam current versus the sample sizes. The linear fitting of $^{12}\text{C}^{3+}$ beam current and the carbon content (%) for three ranges of sample sizes (<20 $\mu\text{g C}$, 20–100 $\mu\text{g C}$, and 100–200 $\mu\text{g C}$) is shown in small figure. The black dots and black line for the range of 100–200 $\mu\text{g C}$, the blue dots and blue line for the range of 20–100 $\mu\text{g C}$, the pink triangles and pink line for the range of <20 $\mu\text{g C}$. (Please see online version for color figures.)

regular 1 mg C targets. For samples of less than 200 $\mu\text{g C}$, the $^{12}\text{C}^{3+}$ beam currents decreased sharply with decreasing sample mass (from 20 μA \rightarrow 1 μA or less), which was primarily attributed to dilution of the carbon concentration in the graphite target (from 25% \rightarrow 1%), and $^{12}\text{C}^{3+}$ beam currents correlated linearly with sample mass. The maximum observed $^{12}\text{C}^{3+}$ beam current to mass ratio was approximately 0.1 $\mu\text{A}/1 \mu\text{g C}$. A relatively uniform distribution of $^{12}\text{C}^{3+}$ beam currents for samples was observed ranging from 20 to 200 $\mu\text{g C}$, and the distribution was linear for samples with masses between 1 and 20 μA . For ultra-small samples of <20 $\mu\text{g C}$, $^{12}\text{C}^{3+}$ beam currents were more dispersed, especially for samples smaller than 10 $\mu\text{g C}$, where the $^{12}\text{C}^{3+}$ beam current was below 1 μA and did not correlate well with sample mass.

By linear fitting of $^{12}\text{C}^{3+}$ beam current and the C% for three sample sizes range (<20 $\mu\text{g C}$, 20–100 $\mu\text{g C}$, and 100–200 $\mu\text{g C}$), it is found that all of them had a strong linear relationship, especially for the sample sizes of 100–200 $\mu\text{g C}$, for which the linear relationship is the most significant ($R^2=0.9894$). These linear relationships become weaker as the sample size decreases,

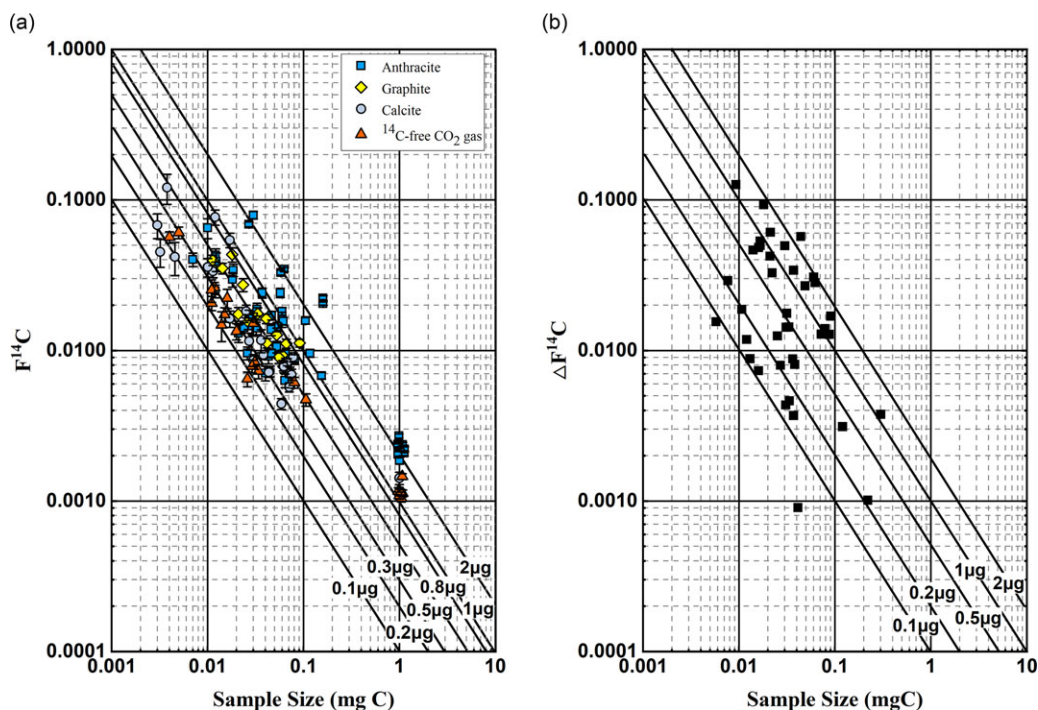


Figure 4 (a) Fraction modern C values for four ^{14}C -free blanks samples from 0.005 mg C to 0.3 mg C sample size are shown to quantify modern carbon contamination (MCC). The four ^{14}C -free blanks represent the MCC from four different processes for the ^{14}C micro-samples analysis: graphitization (^{14}C -free CO_2 gas), surface leaching (carbonates: calcite), combustion and purification (organics: graphite), conventional acid/base/acid washes process (organics: anthracite). (b) $\Delta F^{14}\text{C}$ values for small and ultra-small OxII samples from 0.003 mg C to 1 mg C measured against 1 mg C normalizing OxII standards are shown to quantify the dead carbon contamination (DCC). Note that uncorrected ^{14}C results from smaller OxII samples are always depleted. The solid lines in both plots represent fixed amounts of carbon contamination from 0.1 to 2 μg C.

it is possible that be related to the uncertainty of analytical results caused by the small sample size, the smaller the sample size, the greater the uncertainty introduced into the analytical results. It could be brought on by uncertainties of various apparatus such as pressure gauge, analytical balance, and others. Therefore, a miniature pressure transducer and a 1.2 mL fixed reaction tube are used to minimize this uncertainty of measurement in our reactor, and the uncertainty introduced by this measurement was considered to be small. It is also possible that by the sample purity, the introduction of contamination can also influence the accuracy of sample mass. While the exogenous contamination introduced during the analysis can be solved by taking multiple measurements of different small standard materials at the same time and applying a suitable correction model.

Quantity of Exogenous Carbon Contamination

Exogenous carbon contamination is generally made up of two major components: (1) modern carbon contamination (MCC) and (2) ^{14}C -dead carbon contamination (DCC), both of which are introduced during sample preparation. The contamination can come from chemical reagents, quartz tubes for loading samples, pretreatment protocols, and poor vacuum, and the

uncertainty introduced by this measurement was considered to be small. The proportion of carbon contamination increases as the sample mass decreases, especially for targets with <0.1 mg C, amplifying the effect of contaminations and causing ^{14}C results and $\delta^{13}\text{C}$ data to significantly deviate from true values. A blank correction has become an indispensable step in the analysis of ultra-small samples due to the increased uncertainties associated with ultra-small samples using AMS.

Several researchers have proposed models for this correction calculation. For instance, Santos et al. (2007a) developed formulas to separately correct the contribution of MCC and DCC from unknown samples as small as 0.001 mg C (Santos et al. 2007b, 2010). By analyzing systematic trends of standard and background normalization results from a similar batch, the MCC content was quantified using smaller ^{14}C -free background samples (3–200 μg C) in the same batch. For this purpose, four background materials were analyzed representing four different chemical pretreatment procedures, including anthracite, calcite, and graphite, and ^{14}C -free CO_2 gas (Figure 5a). The trend of the four background $F^{14}\text{C}$ values with varying sample sizes are discussed, the solid lines represent the linear effects of several fixed amounts of MCC contamination ranging from 0.1 to 2 μg C, revealing an average MCC of 0.2–1.2 μg . The fraction modern carbon values of the four backgrounds reflect different sources of MCC contamination introduced from conventional ^{14}C -AMS experimental processes (e.g., acid-base-acid pretreatment of organics, combustion and purification, acid-hydrolysis of carbonates, and graphitization). The estimated quantity of our MCC involving different procedural stages are presented in Table 1. The chemical pretreatment process of ^{14}C -AMS samples must be carefully monitored for ultra-small samples. DCC is calculated from ΔF deviation values of the measured fraction modern carbon for small aliquots OxII samples from the primary standard (1 mg C OxII) (Figure 5b). Similarly, several black solid lines represent the effects of several fixed amounts of DC contamination. Our DC contamination is in the range of 0.1–1.5 μg C.

The MCC of the KCCAMS laboratory was $0.6 \pm 0.3 \mu\text{g}$ C, and DCC was $0.3 \pm 0.15 \mu\text{g}$ C (Santos et al. 2010). The values of the single-stage AMS laboratory at Tokyo University were $0.37 \pm 0.13 \mu\text{g}$ C (MC) and $<1.62 \mu\text{g}$ C (DC) (Masako Yamane et al. 2019). By comparing with data published by other laboratories, it is found that our DC blank contribution was quite significant, this could be attributed to our vacuum system for pumping samples and the chemical reagents used. It is suspected that the use of oil in our vacuum pumps has a negative impact, which, however, needs to be investigated in detail. The ^{14}C content of extraneous carbon in CuO (an oxidation reagent) can vary significantly between batches and suppliers. CuO promotes more contamination than Fe powder (Q. Hua et al. 2004) because more CuO is used for sample preparation, therefore, having a much higher contamination potential. In the future, oil-free pumps and higher purity reagents will be considered to adopt to minimize these contamination contributions during sample processing at the Xi'an AMS center.

Furthermore, we explore the constant contamination model to precisely quantify the $F^{14}\text{C}$ of the contamination ($F^{14}\text{C}_c$) and the mass of the contamination (m_c), the $F^{14}\text{C}$ measured by AMS ($F^{14}\text{C}_m$) can be expressed as:

$$F^{14}\text{C}_m = \frac{F^{14}\text{C}_s \times m_s + F^{14}\text{C}_c \times m_c}{m_m} \quad (1)$$

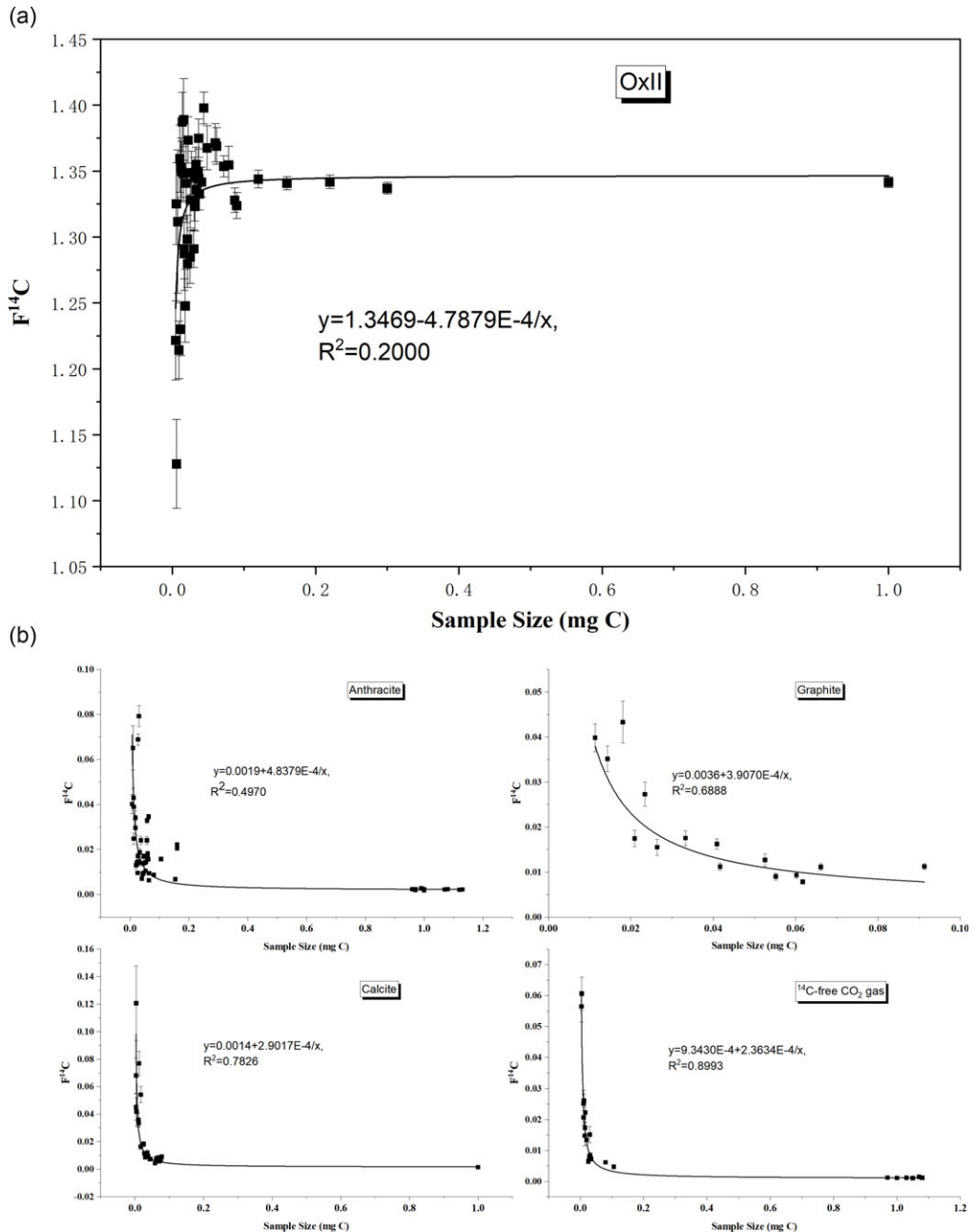


Figure 5 The fitting curves of the reciprocal relationships between our $F^{14}C$ results and sample size for various standards. (a) OxII standards from 0.003 mgC to 1 mgC. All FC results have been corrected for fractionation using $\delta^{13}C$ AMS measurements. (b) Four background materials: anthracite, graphite, calcite, and ^{14}C -free CO_2 gas.

Where the $F^{14}C_s$ is the actual $F^{14}C$ of the sample, and m_m denotes the total measured C mass, which is the sum of the actual mass of the sample (m_s) and m_c . From Equation (1) and derivation, we obtain the following equation:

Table 1 Summary of carbon contamination masses in our ^{14}C -AMS analysis of ultra-small samples.

Background materials	Representative procedural stage	Calculated by method of Hua et al. (2004)		Calculated by method of Santos et al. (2010)	
		$F^{14}\text{C}_c$	$m_c/\mu\text{gC}$	MCC/ μgC	DCC/ μgC
Anthracite	ABA + combustion + graphitization	0.67 ± 0.12	0.72 ± 0.11	0.2–2	
Graphite	Combustion + graphitization	0.60 ± 0.30	0.65 ± 0.11	0.3–0.8	
Calcite	Acid-hydrolyzation + graphitization	0.51 ± 0.19	0.58 ± 0.1	0.2–1	0.1–1.5
^{14}C -free CO_2 gas	Graphitization	0.44 ± 0.09	0.54 ± 0.1	0.2–0.5	

$$F^{14}\text{C}_m = F^{14}\text{C}_s + m_c \times \frac{F^{14}\text{C}_c - F^{14}\text{C}_s}{m_s} \quad (2)$$

The impact of constant contamination is reciprocally related to the sample size, its mass is assumed to be much smaller than that of the sample ($m_c \ll m_s$) (Hua et al. 2004). Since the values of $F^{14}\text{C}_s$, $F^{14}\text{C}_c$ and m_c are constant, $F^{14}\text{C}_m$ is inversely related to m_s , here $F^{14}\text{C}_s$ and $m_c \times (F^{14}\text{C}_c - F^{14}\text{C}_s)$ can be regarded as the offset and coefficient of the $F^{14}\text{C}_m$ and m_s relationships, respectively. The reciprocal curves of OxII and four background samples between our $F^{14}\text{C}_m$ results (corrected for $\delta^{13}\text{C}$ fractionation) and sample size are fitted (Figure 6), and the quantity of our m_c and $F^{14}\text{C}_c$ involved different procedural stages are calculated and presented in Table 1. Based on a two-component mixing model explored in the publication of Hua et al. (2004), the $F^{14}\text{C}$ of our several IAEA reference materials are corrected, the corrected results are illustrated in Figure 8 and discussed in the section ‘‘Accuracy and Reproducibility.’’

Results of $F^{14}\text{C}_c$ and m_c for the different procedural stages of our ^{14}C -AMS analysis are obtained more precisely based on the mass-balance model with the F_c and m_c of the four background standard materials in Table 1. These results include a carbon contamination mass of $0.07 \pm 0.01 \mu\text{g}$ of C with an $F^{14}\text{C}_c$ value of 1.33 ± 0.37 introduced from the acid-base-acid chemical pretreatment process for organics, a mass of $0.11 \pm 0.02 \mu\text{g}$ of C with an $F^{14}\text{C}_c$ value of 1.39 ± 0.37 introduced from the combustion process, a mass of $0.04 \pm 0.008 \mu\text{g}$ of C with an $F^{14}\text{C}_c$ value of 1.36 ± 0.19 introduced from acid-hydrolyzation process for carbonates, and a larger mass of $0.54 \pm 0.10 \mu\text{g}$ of C with an $F^{14}\text{C}_c$ value of 0.44 ± 0.09 introduced from graphitization and AMS measurements process. It is concluded that m_c of graphitization is the most, and more dead carbon contamination is introduced from this process ($F^{14}\text{C} \ll 1$).

Iron catalyst is a key participant in the entire graphitization and AMS measurements, the most probable source of dead carbon contamination can be iron catalyst (Cherkinsky et al. 2013). Correction for contamination of dead and modern carbon which could be present in the catalyst or from cross-contamination in the ion source also plays a significant role, it should not be neglected especially in the ^{14}C -AMS analysis of ultra-small samples ($<20 \mu\text{g C}$). Therefore,

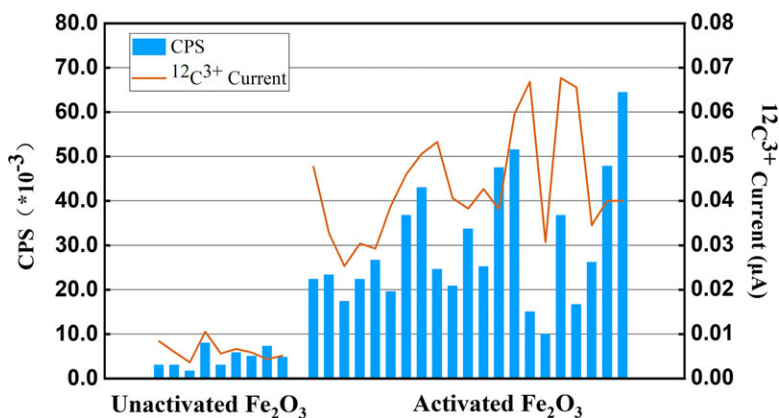


Figure 6 The ^{14}C counts rate (CPS, counts per second) and $^{12}\text{C}^{3+}$ current values of the reagents used in the ultra-small graphite holders. The blue bar chart represented the CPS values of before and after reduced Fe_2O_3 reagents, the brown curves represent $^{12}\text{C}^{3+}$ current values of before and after reduced Fe_2O_3 reagents. The x-axis represents many measurements of targets which were made of Fe and Fe_2O_3 powder in measured wheels.

our measurement results of small samples are performed using a correction method of ^{14}C counts from iron.

Correction of ^{14}C Counts from Fe Powder

In the measured wheels of ultra-small samples, targets made of Fe powder, Nb powder, and Fe_2O_3 were also added. Fe powder and Fe_2O_3 powder were prepared in two ways: (1) pre-activated and (2) post-activated. Pre-activated targets were heated to 600°C for 2 hr. Post-activated targets were reduced with H_2 at 600°C . We measured the ^{14}C count rate and $^{12}\text{C}^{3+}$ beam currents for these targets. The ^{14}C count rate of Fe powder and $^{12}\text{C}^{3+}$ beam currents of the pre-activated and post-activated targets are shown in Figure 7. The ^{14}C count rate and $^{12}\text{C}^{3+}$ beam currents have changed before and after activated Fe_2O_3 . Post-activated targets had higher ^{14}C count rates. This implies that atmospheric $^{14}\text{CO}_2$ (of modern origin) could have contaminated the catalyst during the reaction process. Therefore, we introduce a correction for the exogenous carbon contribution during graphitization by subtracting ^{14}C counts from Fe powder alone. The corrected $F^{14}\text{C}$ was obtained from the subtraction of ^{14}C counts for all samples measured in the same batch respectively, which also includes various standards measured in the same batch the measured, and further calculations with formulas involved in the conventional ^{14}C -AMS analysis.

After correction, $F^{14}\text{C}$ values of the OxII standard and four background materials with various carbon masses are compared with measured values (Figure 7). Figure 7a shows the variation in $F^{14}\text{C}$ values of the OxII standard with varying carbon masses, as well as corrected $F^{14}\text{C}$ values. All results have been corrected for fractionation using $\delta^{13}\text{C}$ -AMS measurements (including machine-induced isotopic fractionation). To precisely clarify the reliability of measurements, the results with three ranges of sample size are analyzed alone. $F^{14}\text{C}$ results ranging from 0.1 mg C to 1 mg C mostly fall on the line of the reference value and lie within the 1σ error of all results of measurements in this range. The average $F^{14}\text{C}$ of 1.3410 ± 0.0051 analyzed the corrected results of sample size with 0.1–1 mg C agrees with the

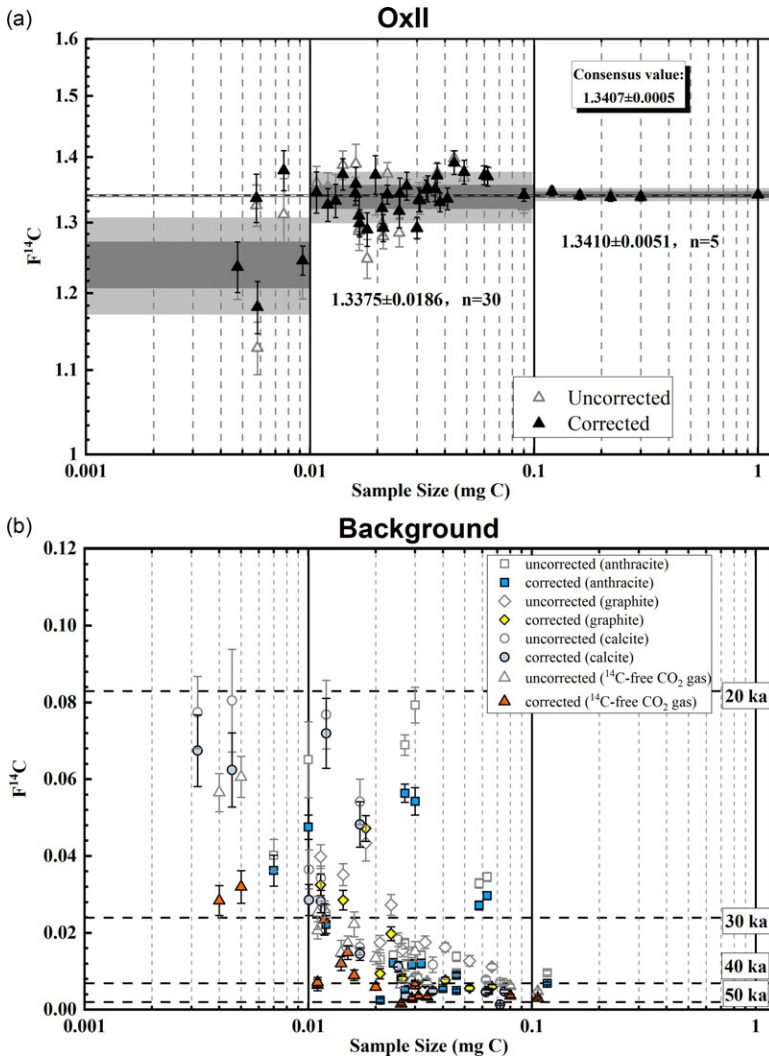


Figure 7 (a) $F^{14}C$ results for multiple ^{14}C -AMS measurements of OxII samples between 0.004 mg C and 1 mg C are shown. The uncorrected $F^{14}C$ values are represented by the black hollow triangle and the corrected $F^{14}C$ values by the black solid triangle. The dashed line represents the consensus value of OxII. The horizontal dark gray (light gray) band indicates the 1σ (2σ) uncertainty calculated from all $F^{14}C$ results corresponding to the range of each sample size. (b) $F^{14}C$ results for background samples between 0.003 mg C and 0.2 mg C from multiple ^{14}C -AMS measurements are shown. The uncorrected $F^{14}C$ values are represented by hollow symbols, and the corrected $F^{14}C$ values by colored solid symbols. Different materials have different symbols and colors: anthracite with square and blue), graphite with Rhombus and yellow, calcite with circle and gray, ^{14}C -free CO_2 gas with triangle and orange. The dashed line represents several ^{14}C age boundaries corresponding to $F^{14}C$ values respectively, including 10 ka, 30 ka, 40 ka, and 50 ka. All results have been corrected for fractionation using $\delta^{13}C$ AMS measurements, also compared the $F^{14}C$ values before and after ^{14}C counts calibrated from Fe powder for all background samples.

consensus value of $F^{14}\text{C} = 1.3407 \pm 0.0005$, with a precision of 3.8‰, which is almost no big difference with of the conventional ^{14}C -AMS analysis. For the range of 0.01–0.1 mg C, the $F^{14}\text{C}$ values have the larger error and are more scattered, $F^{14}\text{C}$ results generally fall within the 2σ error of all results of measurements in this range. The average $F^{14}\text{C}$ of 1.3375 ± 0.0186 ($n = 30$) analyzed the corrected results of sample size with 0.01–0.1 mg C has some deviation from the consensus value of OxII standard, with a precision of 1.39%. For ultra-small samples of <0.01 mg C, improvement range is larger after correction, but the deviation from consensus remains larger. The ^{14}C count correction from Fe powder does not completely solve the correction problem of C contamination for this range, it is implied that preparing samples of <0.1 mg C is very challenging, probably it is necessary to improve the accuracy via strictly controlling the procedural background in the future.

Figure 7b illustrates the variation in $F^{14}\text{C}$ values of all background samples with varying carbon masses, and the corrected background $F^{14}\text{C}$ results. The $F^{14}\text{C}$ values of small background samples increase with decreasing carbon masses. For small samples more than 0.1 mg C, the background ^{14}C ages remain above 40 ka even for ^{14}C -free CO_2 gas close to 50 ka after ^{14}C counts correction. Before the correction, the background ^{14}C results for small samples of 0.1–0.02 mg C generally ranged from 30–40 ka, whereas the ^{14}C results of ^{14}C -free CO_2 gas samples appeared to be higher, mostly around 40 ka; as carbon mass decreases, the background $F^{14}\text{C}$ values gradually increase, with the ^{14}C age of about 30 ka. With correction, extraneous carbon contamination is removed during the graphitization process, resulting in smaller $F^{14}\text{C}$ values and higher background ^{14}C ages, specifically for background gas. For ultra-small samples of <0.02 mg C, the background $F^{14}\text{C}$ values rapidly increase with decreasing carbon masses, which is generally scattered between 20 ka and 35 ka. After correction, the ^{14}C age was close to 40 ka, emphasizing the importance of ^{14}C count correction from Fe powder, which is required urgently for ultra-small samples, specifically those near background levels of less than 0.02 mg C. Consequently, the good agreement of the measurements of OxII and four background standards with their reference values demonstrates the improvement of contamination correction and a good precision of ultra-mass graphite preparation and AMS measurement for small samples of >0.01 mg C at Xi'an AMS center.

Accuracy and Reproducibility

To assess the accuracy and reproducibility of our micro-scale ^{14}C -AMS analysis, we prepared and measured four reference materials from the International Atomic Energy Agency (IAEA), IAEA-C2 (travertine, 7135a BP), IAEA-C3 (cellulose, modern sample), IAEA-C6 (ANU sucrose, modern sample), and IAEA-C7 (oxalic acid, 5644a BP), covering a range of 0.01–0.1 mg C. The IAEA series can help in evaluating different correction methods and measurement performance of small samples. The corrected $F^{14}\text{C}$ values applying three methods for our IAEA reference materials are compared, including (1) the traditional background subtraction: The $F^{14}\text{C}$ values of samples are calculated by the direct subtraction of the $F^{14}\text{C}$ values of background measured in the same batch; (2) the constant contamination model: Based on a two-component mixing model explored in the publication of Hua et al. 2004; and (3) our correction of ^{14}C counts from iron. The three corrected $F^{14}\text{C}$ results with the same sample sizes are illustrated in Figure 8. The corrected results with method (2) are mostly higher than the other corrected results, and the corrected results with method (1) and method (3) are close to each other. In comparison, the corrected $F^{14}\text{C}$ values based on our correction of iron counts are mostly closer to their corresponding consensus values and lie within 1σ uncertainty of all corrected results, which indicates good reproducibility for samples with >0.01 mg of C.

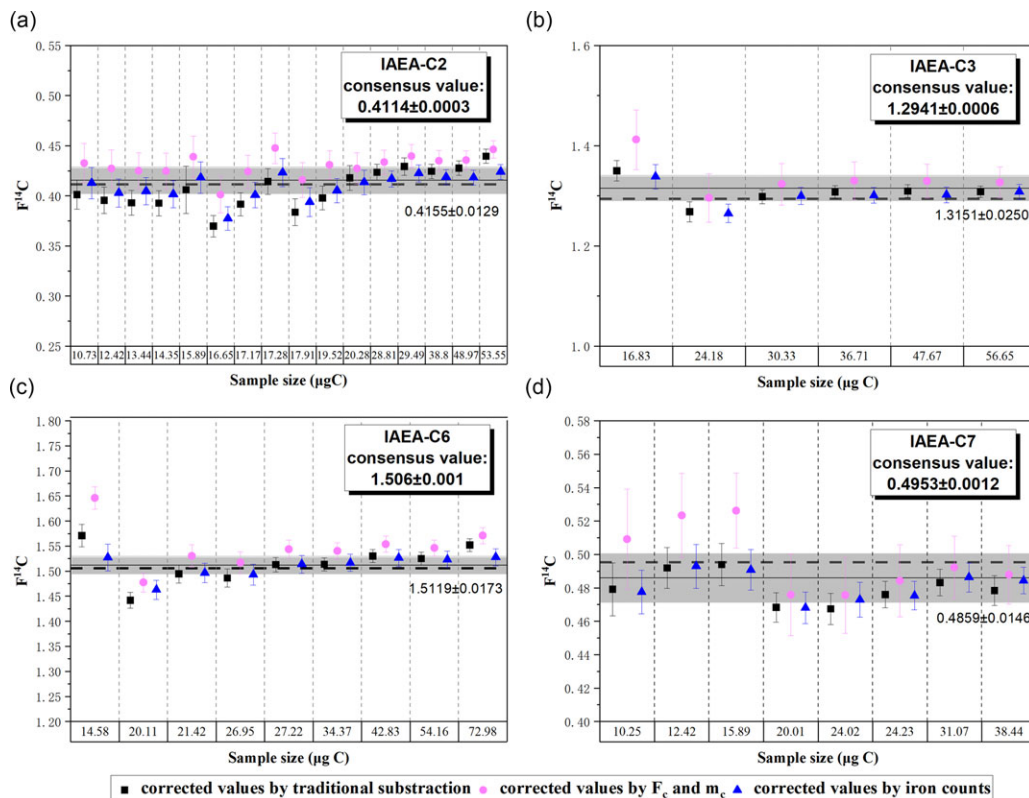


Figure 8 $F^{14}C$ corrected values of IAEA standards ranging 10–100 $\mu\text{g C}$ from multiple ^{14}C -AMS measurements. (a) Different symbols show different correction methods: the traditional background subtraction (black solid squares), constant contamination model (red solid circle), and our correction of ^{14}C counts from iron (blue solid triangle). The black dashed lines represent the $F^{14}C$ consensus values of IAEA standards, the black solid lines and the horizontal gray band represent the average and its associated one-sigma uncertainty of all corrected results.

Overall, ^{14}C analysis of small IAEA reference standard samples containing different sample types and age ranges below 10 ka BP show that our ^{14}C analysis of ultra-small samples of 10–100 $\mu\text{g C}$ obtained accurate and reproducible results.

Case Study

Chronological Framework for Marine Sediment Based on ^{14}C Analysis of Small Foraminiferal Samples

Marine sediments are important scientific carriers for studying major issues including paleoclimate change, sea level trends, and geochemical cycles. Understanding the above issues require a precise chronological frame for marine sediments. Planktonic foraminifera is frequently used as ^{14}C -AMS dating material for marine sediment. We have a collection of foraminifer samples from the South China Sea that have been classified into the genera *G. ruber* and *G. sacculifer*, respectively. We aim to determine a basic chronological sequence for sediment cores from the South China Sea. In practice, there exist few representative and reliable dating materials in sediments, and many harbor exogenous carbon, making the final ^{14}C results unreliable and difficult to interpret. As a result, foraminiferal shells in marine

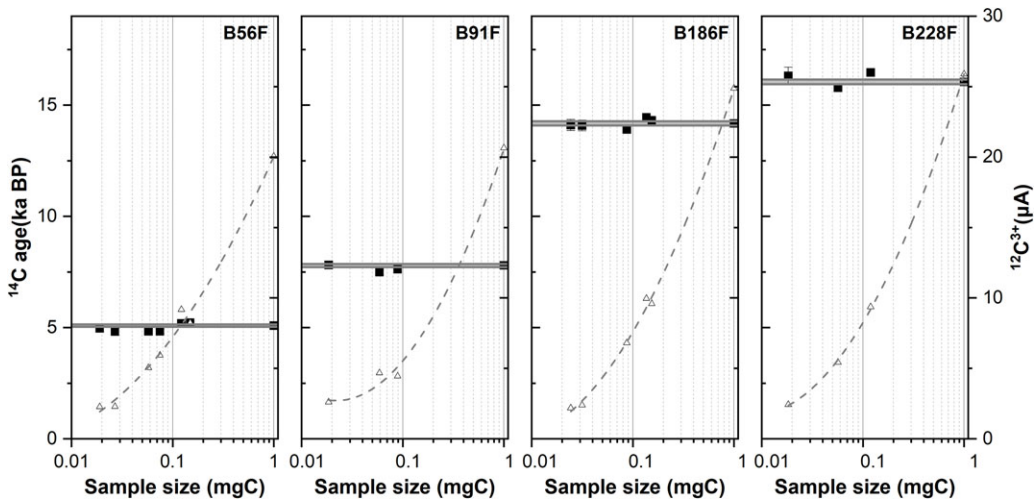


Figure 9 The ^{14}C age results of four foraminifera samples between 10 μgC and 1 mgC from multiple ^{14}C -AMS measurements. All results have been corrected for isotopic fractionation with on-line $\delta^{13}\text{C}$ AMS values and ^{14}C counts of Fe powder. The black solid squares were represented ^{14}C age values and, the black hollow triangles were represented $^{12}\text{C}^{3+}$ beam currents, the gray zones were represented the range of 3σ errors of ^{14}C age of 1 mg C sample, the dotted lines were represented the linear relationship between $^{12}\text{C}^{3+}$ currents and the sample size.

sediments are selected for dating; it is even more crucial to select a single species of foraminifera for accurate dating. Nevertheless, the quality of single species of foraminifera that can be obtained is frequently limited. Therefore, establishing a chronological framework of marine sediment cores requires reliable ^{14}C -AMS analysis of small foraminifer samples, even ultra-small samples.

In the first stage, four high-quality foraminifer samples were selected for analysis, i.e., 110–112 cm (B56F), 180–182 cm (B91F), 370–372 cm (B186F), and 453–455 cm (B228F). Through carbonate hydrolysis pretreatment, each sample was separated into many small samples of CO_2 (0.01–0.2 mg C) for graphitization and AMS dating. Meanwhile, we prepared 1 mg C graphite of each foraminifer sample for AMS measurement to study if ultra-small foraminifera samples as low as 0.01 mg C could be precisely dated as 1 mg C samples. As shown in Figure 9, the ^{14}C -AMS outcomes of small foraminifer samples have been corrected for isotopic fractionation with $\delta^{13}\text{C}$ -AMS values and ^{14}C counts of Fe powder. In contrast with the ^{14}C ages of the 1 mg C sample as the reference values, the ^{14}C ages of the four foraminifer samples were all dispersed around the corresponding reference values and are within the 3σ error range of the reference value, which is comparable with the ^{14}C results of 1 mg C sample. This illustrates that our small foraminifer samples of 10–200 μgC can also yield stable and reliable ^{14}C ages, which can help in the dating of important layers lacking effective C fractions and emphasize the importance of correctly constructing the chronological framework of marine sediment cores.

CONCLUSIONS

Accurate and reproducible ^{14}C analyses in small samples containing 10–300 μgC were accomplished using the developed micro-specific graphitization reactors and the ^{14}C -AMS analysis of ultra-small graphite targets. The following conclusions are obtained:

1. For samples containing less than 200 $\mu\text{g C}$, a good linear correlation between $^{12}\text{C}^{3+}$ beam current and sample mass was observed, which corresponded to the maximum $^{12}\text{C}^{3+}$ beam current of approximately 0.1A/ μgC in our facility.
2. The analysis of Modern and ^{14}C -dead carbon contamination revealed that the total MCC for small samples was 0.2–1.2 $\mu\text{g C}$, whereas the DCC was 0.1–1.5 $\mu\text{g C}$. Moreover, $F^{14}\text{C}_c$ and m_c for four background standard materials are obtained more precisely based on the constant contamination model. The results reveal that m_c of graphitization and AMS measurements is the most significant, and more dead carbon contamination is introduced from this process ($F^{14}\text{C} \ll 1$).
3. The good agreement of the measurements of OxII and four background standards with their reference values demonstrates the improvement of contamination correction and a good precision of ultra-mass graphite preparation and AMS measurement for small samples of >0.01 mg C at Xi'an AMS center, especially for ultra-small ^{14}C -free CO_2 gas samples of >0.02 mg C, where the ^{14}C age limitation is approximately 40 ka BP.
4. ^{14}C analysis of small IAEA reference standard samples containing different sample types and age ranges below 10 ka BP was performed, and small foraminifer samples were analyzed and discussed to establish a chronological sequence for marine sediment. Both analyses showed that our ^{14}C analysis of ultra-small samples of 10–100 $\mu\text{g C}$ obtained accurate and reproducible results.

The developed micro-scale ^{14}C -AMS analysis technique proved useful for research applications requiring high-precision dating and tracer applications, acting as a supplement to the conventional ^{14}C -AMS analysis at the mg C level. Ultra-small samples of <10 $\mu\text{g C}$ will be examined in the future.

ACKNOWLEDGMENTS

We are grateful to Dr. Bin Yang for the installation of the micro-specific graphitization reactor. This work was supported by the Strategic Priority Research Program of the Chinese Academy of Sciences (B) (Grant No. XDB40000000), West Light Foundation of the Chinese Academy of Sciences (Grant No. XAB2022000008), the Natural Science Basic Research Program of Shaanxi (Grant No. 2022000017) and Youth Innovation Promotion Association CAS (Grant No. Y2021108).

REFERENCES

- Berstan R, Stott AW, Minnitt S, Ramsey BC, Hedges REM, Evershed RP. 2008. Direct dating of pottery from its organic residues: new precision using compound specific carbon isotopes. *Antiquity* 82:702–713.
- Buchholz BA, Spalding KL. 2010. Year of birth determination using radiocarbon dating of dental enamel. *Surf Interface Anal.* 42(5):398–401. doi: [10.1002/sia.3093](https://doi.org/10.1002/sia.3093)
- Casanova E, Knowles TDJ, Bayliss A, Dunne J, Barański MZ, Denaire A et al. (2020). Accurate compound-specific ^{14}C dating of archaeological pottery vessels. *Nature* 580:506–510.
- Cherkinsky A., Prasad G.V. R., Dvoracek D.K. 2013. AMS measurement of samples smaller than 300 μg at Center for Applied Isotope Studies, University of Georgia. *Nuclear Instruments and Methods in Physics Research Section B* 294:87–90.
- Cook GT, Dunbar E, Black SM, Xu S. 2006. A preliminary assessment of age at death determination using the nuclear weapons testing ^{14}C activity of dentine and enamel. *Radiocarbon* 48:305–313.
- Devièse T, Stafford TW, Waters MR, Wathen C, Comeskey D, Becerra-Valdivia L, Higham T. 2018. Increasing accuracy for the radiocarbon dating of sites occupied by the first Americans. *Quaternary Science Reviews* 198:171–180.
- Druffel ERM, Zhang D, Xu X, Ziolkowski LA, Southon JR, Santos GM, Trumbore SE. 2010.

- Compound-specific radiocarbon analyses of phospholipid fatty acids and n-alkanes in ocean sediments. *Radiocarbon* 52(2–3):1215–1223.
- Eglinton TI, Aluwihare LI, Bauer JE, Druffel ERM, McNichol AP. 1996. Gas chromatographic isolation of individual compounds from complex matrices for radiocarbon dating. *Analytical Chemistry* 68:904–912.
- Fahrni SM, Wacker L, Synal HA, Szidat S. 2013. Improving a gas ion source for ^{14}C AMS. *Nuclear Instruments and Methods in Physics Research B* 294:320–327.
- Feng XJ, Vonk JE, Griffin C, Zimov N, Montluçon DB, Wacker L, Eglinton TI. 2017. C variation of dissolved lignin in arctic river systems. *ACS Earth and Space Chemistry* 1(6):334–344.
- Fu YC, Zhou WJ, Du H, Cheng P, Zhao XL, Liu Q, Lu XF, Zhao WN. 2015. A preliminary study of small-mass radiocarbon sample measurement at Xi'an-AMS. *Chinese Physics C* 39(3):036202.
- Hippe K, Jansen JD, Skov DS et al. 2021. Cosmogenic in situ ^{14}C - ^{10}Be reveals abrupt Late Holocene soil loss in the Andean Altiplano. *Nature Communication* 12:2546.
- Hippe K, Kober F, Baur H, Ruff M, Wacker L, Wieler R. 2009. The current performance of the in situ ^{14}C extraction line at ETH. *Quaternary Geochronology* 4:493–500.
- Hua Q, Zoppi U, Williams AA, Smith AM. 2004. Small-Mass AMS Radiocarbon Analysis at ANTARES. *Nuclear Instruments and Methods in Physics Research B* 223–224:284–292.
- Kim SH, Kelly PB, Clifford AJ. 2008. Biological/biomedical accelerator mass spectrometry targets. 2. Physical, morphological, and structural characteristics. *Analytical Chemistry* 80:7661–7669.
- Liebl J, Steier P, Golser R, Kutschera W, Mair K, Priller A, Vonderhaid I, Wild EM. 2013. Carbon background and ionization yield of an AMS system during ^{14}C measurements of microgram-size graphite samples. *Nuclear Instruments and Methods in Physics Research Section B* 294:335–339.
- Lifton NA, Jull AJT, Quade J. 2001. A new extraction technique and production rate estimate for in-situ cosmogenic ^{14}C in quartz. *Geochimica et Cosmochimica Acta* 65(12):1953–1969.
- Lupkera M, Hippe K, Wacker L, Steinemann O, Tikhonirov D, Madene C, Haghipoura N, Synal HA. 2019. In-situ cosmogenic ^{14}C analysis at ETH Zürich: Characterization and performance of a new extraction system. *Nuclear Instruments and Methods in Physics Research Section B* 457:30–36.
- Melchert J, Stolz A, Dewald A, Gierga M, Wischhöfer P, Rethemeyer J. 2019. Exploring sample size limits of AMS gas ion source ^{14}C analysis at CologneAMS. *Radiocarbon* 61(6):1785–1793. doi: [10.1017/RDC.2019.143](https://doi.org/10.1017/RDC.2019.143)
- Miller GH, Briner JB, Lifton NA, Finkel RC. 2006. Limited ice-sheet erosion and complex exposure histories derived from in situ cosmogenic ^{10}Be , ^{26}Al , and ^{14}C on Baffin Island, Arctic Canada. *Quaternary Geochronology* 1(1):74–85.
- Pigati JS, Lifton NA, Jull AJT, et al. 2010. A simplified in-situ cosmogenic ^{14}C extraction system. *Radiocarbon* 52(2–3):1236–1243.
- Pearson A, McNichol AP, Schneider RJ, Von Reden KF and Zhang Y. 1998. Microscale AMS ^{14}C measurement at NOSAMS. *Radiocarbon* 40(1):61–75.
- Ruff M, Szidat S, Gäggeler HW, Suter M, Synal HA, Wacker L. 2010. Gaseous radiocarbon measurements of small samples. *Nuclear Instruments and Methods in Physics Research B* 268:790–794.
- Ruff M, Wacker L, Gäggeler HW, Suter M, Synal HA, Szidat S. 2007. A gas ion source for radiocarbon measurements at 200 kV. *Radiocarbon* 49:307–314.
- Saitoh H, et al. 2019. Estimation of birth year by radiocarbon dating of tooth enamel: approach to obtaining enamel powder. *Journal of Forensic and Legal Medicine* 62:97–102.
- Salehpour M, Håkansson K, Possnert G. 2013. Accelerator mass spectrometry of ultra-small samples with applications in the biosciences. *Nuclear Instruments and Methods in Physics Research B* 294:97–103.
- Santos GM, Moore RB, Southon JR, Griffin S, Hinger e, Zhang D. 2007a. AMS ^{14}C sample preparation at the KCCAMS/UCI facility: status report and performance of small samples. *Radiocarbon* 49(2):255–269.
- Santos GM, Southon JR, Griffin S, Beupre SR, Druffel ERM. 2007b. Ultra small-mass AMS ^{14}C sample preparation and analyses at KCCAMS/UCI Facility. *Nuclear Instruments and Methods in Physics Research B* 259:293–302.
- Santos GM, Southon JR, Drenzek NJ, Ziolkowski LA, Druffel ERM, Xu XM, Zhang D, Trumbore S, Eglinton TI, Hughen KA. 2010. Blank assessment for ultra-small radiocarbon samples: chemical extraction and separation versus AMS. *Radiocarbon* 52(2–3):1322–1335.
- Smith AM, Hua Q, Williams A, Levchenko V, Yang B. 2010. Developments in micro-sample ^{14}C -AMS at the ANTARES AMS facility. *Nuclear Instruments and Methods in Physics Research B* 268(7–8):919–923.
- Smith AM, Hua Q, Williams AA, Thorpe KJ. 2006. A novel laser-heated microfurnace for the preparation of microgram-sized AMS graphite targets. 19th International Radiocarbon Conference. Oxford, 3–7 April 2006. Oxford, UK.
- Spalding KL, Arner E, Westermark PO, Bernard S, Buchholz BA, Bergmann O, et al. 2008. Dynamics of fat cell turnover in humans. *Nature* 453:783–787.

- Spalding KL, Bergmann O, Alkass K, Bernard S, Salehpour M, Huttner HB, Bostro E, Westerlund I, et al. 2013. Dynamics of hippocampal neurogenesis in adult humans. *Cell* 153(6): 1219–1227.
- Steier P, Liebl J, Kutschera W, Wild EM, Golser R. 2017. Preparation methods of μg carbon samples for ^{14}C measurements. *Radiocarbon* 59(3):803–814.
- Spindler L, Comeskey D, Chabai V, Uthmeier T, Buckley M, Deviese T, Higham T. 2021. Dating the last Middle Palaeolithic of the Crimean Peninsula: new hydroxyproline AMS dates from the site of Kabazi II. *Journal of Human Evolution* 156:102996.
- Uhl T, Luppold W, Rottenbach A, Scharf A, Kritzler K, Kretschmer W. 2007. Development of an automatic gas handling system for microscale AMS ^{14}C measurements. *Nuclear Instruments and Methods in Physics Research B* 259:303–307.
- Walker BD, Xu XM. 2019. An improved method for the sealed-tube zinc graphitization of microgram carbon samples and ^{14}C AMS measurement. *Nuclear Instruments and Methods in Physics Research B* 438:58–65.
- Walter SRS, Gagnon AR, Roberts ML, McNichol AP, Gaylord MCL, Klein E. 2015. Ultra-small graphitization reactors for ultra-microscale ^{14}C analysis at the national ocean sciences accelerator mass spectrometry (NOSAMS) facility. *Radiocarbon* 57(1):109–122.
- Welte C, Hendriks L, Wacker L, Haghypour N, Eglinton TI, Günther D, Synal HA. 2018. Towards the limits: analysis of microscale ^{14}C samples using EA-AMS. *Nuclear Instruments and Methods in Physics Research Section B* 437:66–74.
- Xu X, Gao P, Salamanca EG. 2013. Ultra small-mass graphitization by sealed tube zinc reduction method for AMS ^{14}C measurements. *Radiocarbon* 55:608–616.
- Yamane M, Yokoyama Y, Hirabayashi S, Miyairi Y, Ohkouchi N, Aze T. 2019. Small- to ultra-small-scale radiocarbon measurements using newly installed single-stage AMS at the University of Tokyo. *Nuclear Instruments and Methods in Physics Research Section B* 455:238–243.
- Yang B, Smith AM. 2017. Conventionally heated microfurnace for the graphitization of microgram-sized carbon samples. *Radiocarbon* 59(3):859–873.
- Yang B, Smith AM, Hua Q. 2013. A cold finger cooling system for the efficient graphitisation of microgram-sized carbon samples. *Nuclear Instruments and Methods in Physics Research B* 294:262–265.
- Yokoyama Y, Koizumi M, Matsuzaki H, Miyairi Y, Ohkouchi N. 2010. Developing ultra small-scale radiocarbon sample measurement at the university of Tokyo. *Radiocarbon* 52(2–3): 310–318.
- Zhang YM, Huang XY, Xie SC. 2021. Compound specific carbon isotope composition of microbial phospholipid fatty acids reveal carbon cycling processes. *Quaternary Sciences* 41(4):877–892.
- Zhao MX, Meng Y, Zhang HL, Tao SQ. 2014. Applications of compound-specific radiocarbon analysis in oceanography and environmental science. *Acta Oceanologica Sinica* 36(4):1–10. In Chinese.
- Zhou W, Lu X, Wu Z, Zhao W, Huang C, Li L, Cheng P, Xin Z. 2007. New results on Xi'an-AMS and sample preparation systems at Xi'an-AMS center. *Nuclear Instruments and Methods in Physics Research Section B* 262:135–142.
- Zhou W, Wu S, Lange T, Lu X, Cheng P, Xiong X, Cruz R, Liu Q, Fu Y, Zhao W. 2012. High-level ^{14}C contamination and recovery at Xi'an AMS Center. *Radiocarbon* 54(2):187–193.
- Zhou W, Zhao X, Lu X, Liu L, Wu Z, Cheng P, Zhao W, Huang C. 2006. The 3MV Multi-Element AMS in Xi'an, China: unique features and preliminary tests. *Radiocarbon* 48(2): 285–293.